Journal of Alloys and Compounds 509 (2011) 4092–4097

Contents lists available at ScienceDirect

Journal of Alloys and Compounds

journal homepage: www.elsevier.com/locate/jallcom

Thermal stability of heavily drawn Cu–0.4 wt.%Cr–0.12 wt.%Zr–0.02 wt.%Si–0.05 wt.%Mg

X.F. Li[a], A.P. Dong[b], L.T. Wang[b], Z. Yu[b], L. Meng[a,*]

[a] Department of Materials Science and Engineering, Zhejiang University, Hangzhou 310027, China
[b] China Railway Electrification Bureau Group Co., Ltd., Beijing 100036, China

ARTICLE INFO

Article history:
Received 3 April 2010
Received in revised form 20 May 2010
Accepted 30 May 2010
Available online 11 June 2010

Keywords:
Metals and alloys
Microstructure
X-ray diffraction
Mechanical properties
Thermal analysis

ABSTRACT

Cu–0.4 wt.%Cr–0.12 wt.%Zr–0.02 wt.%Si–0.05 wt.%Mg was prepared by casting, quenching, aging and cold drawing. The microstructure was studied by electron microscope and X-ray diffraction. Vickers hardness was measured for the alloy after the annealing treatment at different temperatures covering a wide temperature range from room temperature to 700 °C. The ribbonlike structure is replaced by gross equiaxed grains. The crystal orientation is gradually approaching the full annealed specimen and the hardness difference between longitudinal and transverse directions vanishes by recovery and recrystallization. The thermal analysis was carried out and the stored energy was calculated. The release of stored energy and the reduction of resistivity are primarily due to the decrease of dislocation density. The main strengthening effect is attributed to dislocation mechanism.

© 2010 Elsevier B.V. All rights reserved.

1. Introduction

Cu–Cr–Zr alloys are widely used in engineering applications, such as trolley wires, lead frames, electronic terminals and connectors due to their high mechanical strength, electrical conductivity, thermal conductivity and wear resistance [1–4]. Many researches have focused on the microstructure [5–9], physical properties and mechanical behavior of the alloys [10–17].

Heavy cold deformation can induce high strength for the alloys due to the strain-hardening effect. However, the strain-hardening effect can be removed during the heat treatment process by the release of the stored deformation energy in recovery and recrystallization, which results in the change of the microstructure and properties of the deformed alloys. Therefore, the stability of a deformed alloy during heat treatment process usually plays an important role in the microstructure and properties. The thermal stability dependent on the stored energy was related to the amount of dislocations and their spatial structure formed during cold deformation [18]. Some studies on the thermal stability or recrystallization behavior related to the release of the stored energy in polycrystalline metals and alloys with heavy plastic deformation have been presented. In cold rolling Al–2.5 wt.%Mg, the release of the stored energy was dependent on the annihilation of defects during recrystallization and the desegregation of solute atoms from the core of dislocations. The dissolution of Mg clusters formed in dislocation walls resulted in an endotherm behavior at low temperatures [19]. Ref. [20] indicated that the stored energy was independent of rolling temperature in Al–Mg–Si alloy due to the higher stacking fault energy of the alloy compared to Cu. The stored energy in high purity copper increased with increasing strain degree and reached a saturation corresponding to a nearly constant recrystallization temperature after a critical strain level [21,22]. In shock-deformed Cu and Cu–Al alloys, the stored energy released during recrystallization was attributed primarily to the annihilation of dislocation with the energy contribution from recovery, deformation twins and point defects estimated to be relatively small [23,24]. The dislocation density was calculated by the total stored energy released during recrystallization and corresponded to a reasonable flow stress in cold rolled pure Cu and Fe [25,26]. In ultrafine-grained metals and alloys, the majority of stored energy released during recrystallization is not only due to the disappearance of dislocations, but also the annihilation of high density grain boundaries. Ref. [27] indicated the Cu power stored about 1.2 kJ/mol and the Ta power about 8 kJ/mol by high energetic ball milling in Cu–Ta alloys. Increasing the grain size decreased the amount of the stored energy at a given strain and increased the recrystallization temperature in pure nickel [28].

There should be high dislocation density and high stored energy in Cu–Cr–Zr alloys with high strength induced by heavy cold deformation. The high stored energy must affect the thermal stability of the microstructure and properties. The aim of the current investigation is to understand the thermal stability

* Corresponding author. Tel.: +86 57187951027; fax: +86 57187952290.
E-mail address: mengliang@zju.edu.cn (L. Meng).

0925-8388/$ – see front matter © 2010 Elsevier B.V. All rights reserved.
doi:10.1016/j.jallcom.2010.05.166

of Cu–Cr–Zr alloys with heavy cold deformation. For the aim, Cu–0.4 wt.%Cr–0.12 wt.%Zr–0.02 wt.%Si–0.05 wt.%Mg was drawn to a high strain degree and then annealed at different temperatures. The recrystallization behavior was studied by microstructure observation, structure analysis, hardness test and resistivity measurement. The stored energy was measured and utilized to estimate dislocation density and flow stress.

2. Experimental methods

Cu–0.4 wt.%Cr–0.12 wt.%Zr–0.02 wt.%Si–0.05 wt.%Mg was melted in a vacuum induction furnace and cast into cylindrical ingots of 20 mm diameter in Ar shielded atmosphere. The ingots were drawn at ambient temperature into wire specimens with the true strain $\eta = 6.0$. The wire specimens were annealed in a vacuum resistance furnace for 1 h at different temperatures.

The microstructure on longitudinal section of the wire specimens was observed by scanning electron microscopy (SEM) and transmission electron microscope (TEM) on a JEM 2010 instrument operated at 200 kV. TEM foils were sliced from the longitudinal section. Then the foils were prepared by a double jet electropolisher at about −20 °C with an electrolyte of 10% nitric acid and 90% methanol. The hardness was determined on polished longitudinal and transverse sections of the wire specimens using a Vickers hardness tester with a load of 200 g and a holding time of 10 s. The hardness value for each sample was taken from the measured average of at least 10 indentations. The electrical resistivity was measured at ambient temperature by the four-probe direct current technique. The flow stress was determined by electronic tensile tester with the strain rate of $2.0 \times 10^{-3}\ s^{-1}$. X-ray diffraction (XRD) analysis was conducted with CuK_α radiation ($\lambda = 0.154$ nm). The microstrain was calculated by the analysis of XRD peak broadening. The thermal analysis was carried out by differential scanning calorimetry (DSC) with a heating rate of 20 °C/min from 40 to 600 °C. The stored energy was taken as the area under the heat releasing peak. For each sample, two DSC runs were obtained and the curve from the second run was used as a baseline. The final DSC curve is the difference between the second run and the first run. Such a procedure is necessary to amplify the extremely small thermal events that occur in Cu–0.4 wt.%Cr–0.12 wt.%Zr–0.02 wt.%Si–0.05 wt.%Mg with heavy deformation.

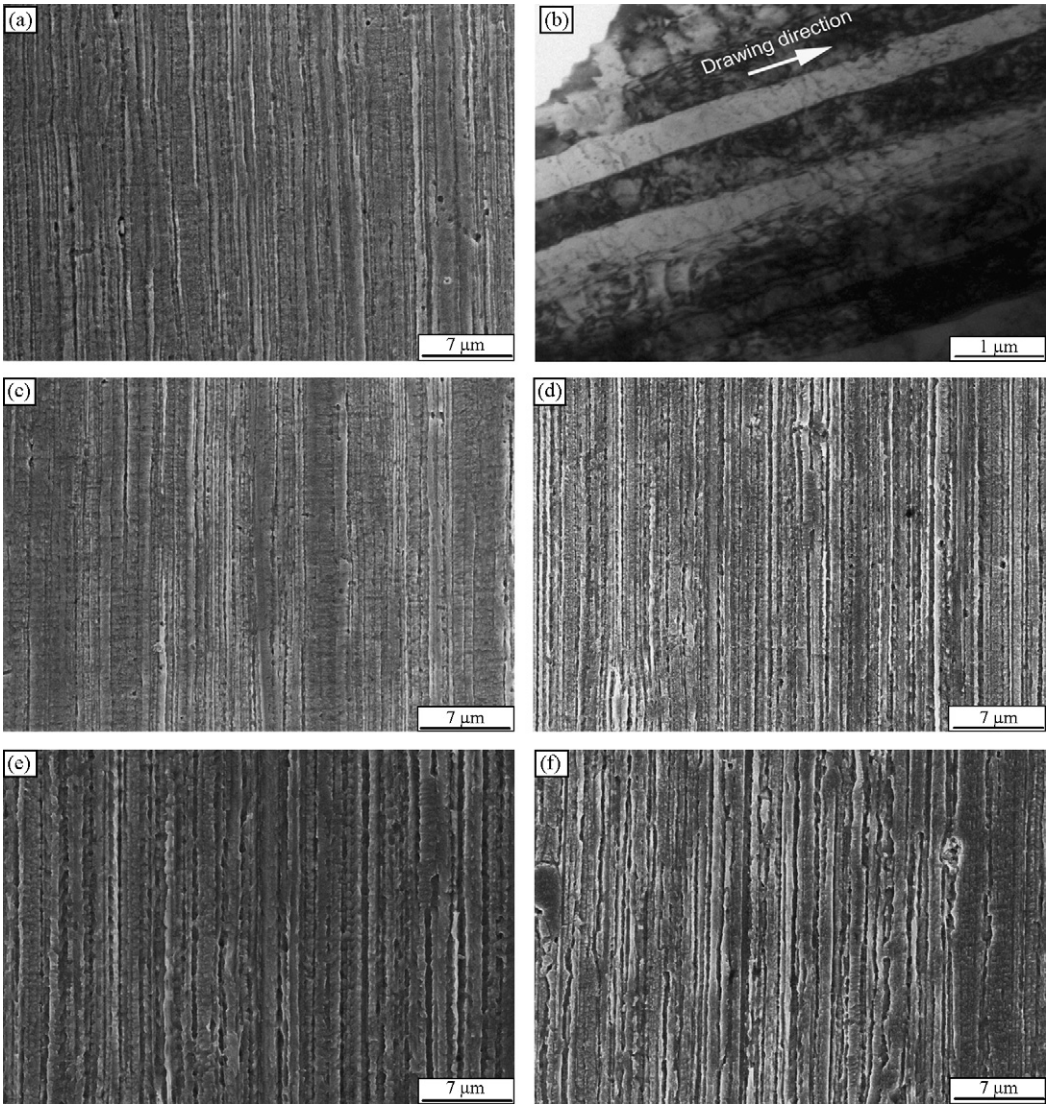

Fig. 1. Microstructure of Cu–0.4 wt.%Cr–0.12 wt.%Zr–0.02 wt.%Si–0.05 wt.%Mg drawn to $\eta = 6.0$ (a) SEM image, (b) TEM image and annealed at (c) 300, (d) 400, (e) 450, (f) 500, (g) 550, (h) 600 and (i) 700 °C.

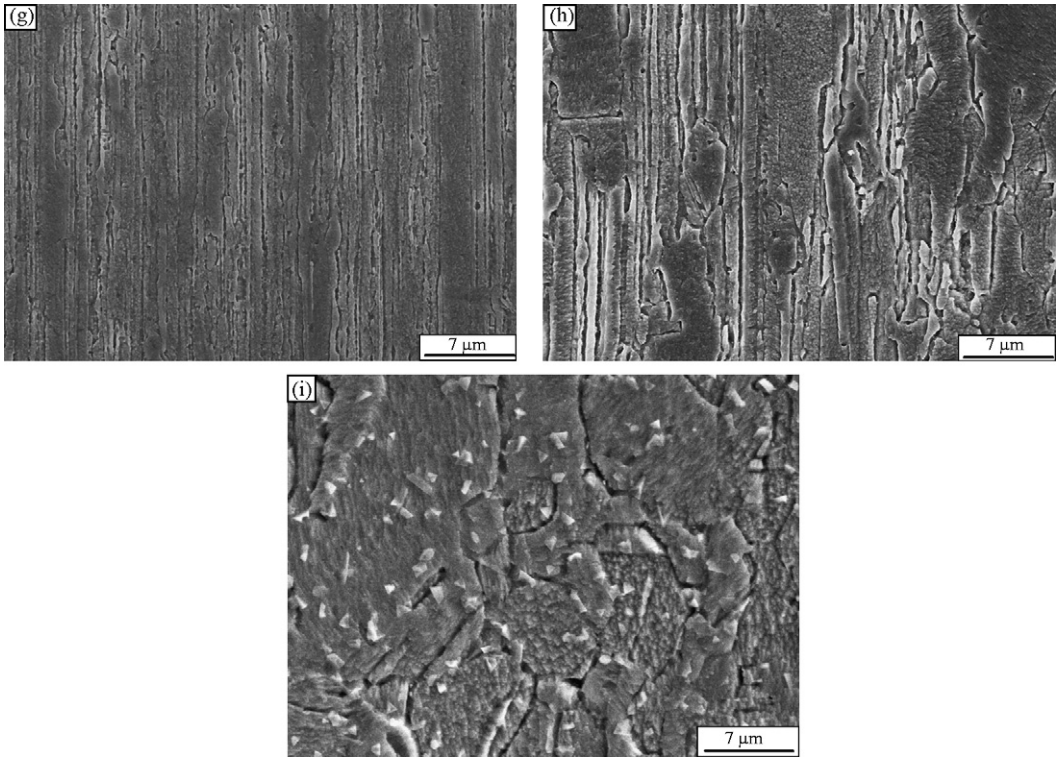

Fig. 1. (*Continued*).

3. Experimental results and discussion

3.1. Microstructure

Fig. 1 shows the microstructure of Cu–0.4 wt.%Cr–0.12 wt.%Zr–0.02 wt.%Si–0.05 wt.%Mg drawn to $\eta = 6.0$ and then annealed at different temperatures. The as-drawn microstructure displays the uniform ribbonlike grains elongated along drawing direction with a mean ribbon diameter of 530 nm. The ribbonlike structure is still retained in the alloy annealed at 300 °C. Some small granular grains form due to the presence of recrystallization in the ribbons annealed at 400 °C and some ribbonlike boundaries slightly migrate. The number of granular grains increases and the migration of ribbonlike boundaries becomes more obvious in the specimens annealed at 450 °C. More obvious migration of ribbonlike boundaries takes place in the specimens annealed at 500 °C. Annealing at 550 °C produces obviously tortuous boundaries and some coalescent ribbons due to further boundary migration at higher temperature. Coarse equiaxed grains across several ribbons are observed and result in the partial disappearance of ribbonlike morphology in the specimens annealed at 600 °C. Considerable grain growth takes place and the ribbonlike morphology completely vanishes away in the specimens annealed at 700 °C.

3.2. Structure evolution

Fig. 2 shows the XRD patterns of Cu–0.4 wt.%Cr–0.12 wt.%Zr–0.02 wt.%Si–0.05 wt.%Mg annealed at different temperatures. The XRD patterns not only show the peak distribution of Cu phase but also the relative intensities of peaks change with the annealing temperature. For example, the $(2\,2\,0)_{Cu}$ intensity is the highest in the as-drawn specimens but decreases with the annealing temperature increasing. On the contrary, the $(1\,1\,1)_{Cu}$ intensity is the lowest in the as-drawn specimens but increases with the annealing temperature increasing. These results imply that the annealing treatment results in the change of crystal orientation in the annealed alloy.

The degree of preferred orientation can be calculated by using the Lotgering factor [29]

$$L_{(hkl)} = (P_{(hkl)} - P^0_{(hkl)})/(1 - P^0_{(hkl)}) \quad (1)$$

$$P_{(hkl)} = I_{(hkl)} / \sum_j I_j \quad (2)$$

$$P^0_{(hkl)} = I^0_{(hkl)} / \sum I^0_j \quad (3)$$

where $I_{(hkl)}$ and $I^0_{(hkl)}$ are the intensities of (hkl) diffraction in the drawn specimen and full annealed specimen, and I_j and I^0_j

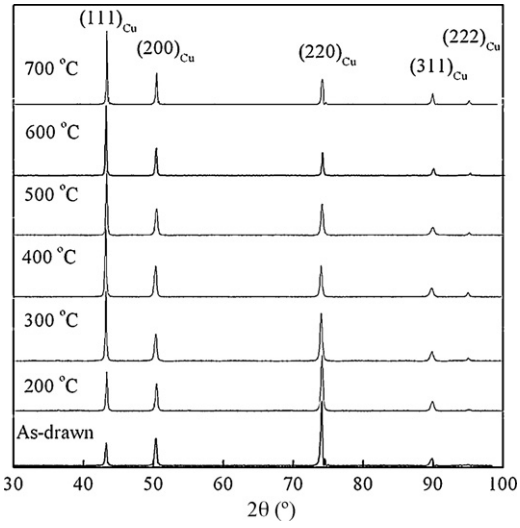

Fig. 2. XRD patterns from longitudinal section of Cu–0.4 wt.%Cr–0.12 wt.%Zr–0.02 wt.%Si–0.05 wt.%Mg drawn to $\eta = 6.0$ and annealed at different temperatures.

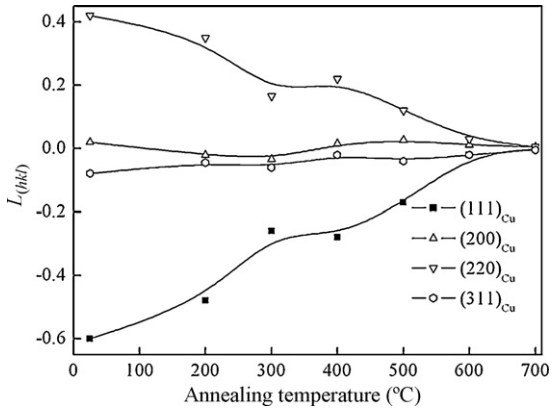

Fig. 3. Lotgering factor dependent on the annealing temperature for Cu–0.4%Cr–0.12%Zr–0.02%Si–0.05%Mg drawn to $\eta = 6.0$.

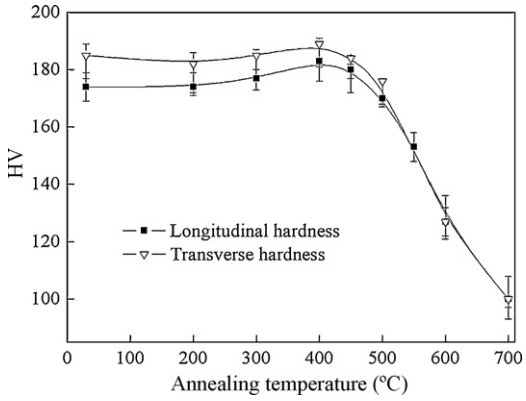

Fig. 5. Vickers hardness dependent on the annealing temperature for Cu–0.4%Cr–0.12%Zr–0.02%Si–0.05%Mg drawn to $\eta = 6.0$.

the intensities of any diffraction in the drawn specimen and full annealed specimen, respectively. The difference of crystal orientation between drawn specimen and full annealed specimen can be reflected by the absolute value of $L_{(hkl)}$. It is obvious that there is the same crystal orientation between the drawn specimen and the full annealed specimen if $L_{(hkl)} = 0$. In general, the greater the absolute value of $L_{(hkl)}$, the higher the difference of the crystal orientation.

Fig. 3 shows the Lotgering factors of different diffractions for the alloy drawn and annealed at different temperatures, where $I^0_{(hkl)}$ and I^0_j are taken from the XRD pattern of the specimen annealed at 700 °C. The crystal orientation of as-drawn specimen has relatively high difference with the annealed specimen. With the annealing temperature increasing, the difference decreases and almost vanishes as the annealing temperature to 600 °C. Fig. 4 shows the microstrain dependent on the annealing temperature. The XRD pattern of the annealed Cu has been used as the standard pattern without microstrain for the calculation of the microstrain. There is a high degree of microstrain in the heavily drawn specimen. With the annealing temperature increasing to 400 °C, the microstrain slowly decreases because the stored energy is released to a certain degree and the internal stress is partially relaxed by the recovery. As the annealing temperatures is higher than 400 °C, the microstrain decreases rapidly because the stored energy is completely released or the dislocation density is dramatically decreased in the recrystallization. Previous investigations showed that microstrain in high purity Cu samples processed by different approaches varied in a wide range, such as 0.1% in equal-channel angular pressing Cu [30], 0.2% in ball-milled Cu [31], 0.24% in magnetron sputtering Cu [32] and 0.16% in conventional cold rolling Cu [25]. The present

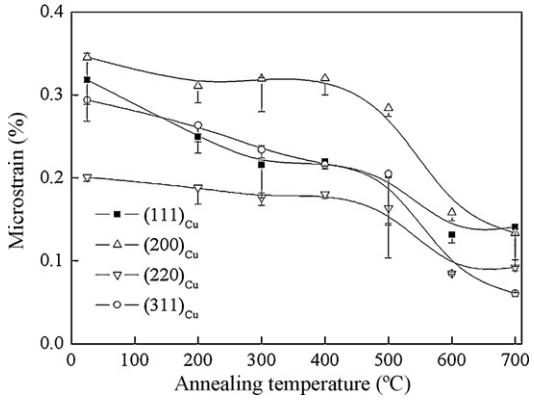

Fig. 4. Microstrain dependent on the annealing temperature for Cu–0.4 wt.%Cr–0.12 wt.%Zr–0.02 wt.%Si–0.05 wt.%Mg drawn to $\eta = 6.0$.

results are slightly higher than those reported in the literature due to the alloying which includes solid solution and precipitation as well as their interactions with dislocations [20,33–36].

3.3. Hardness

Fig. 5 shows the hardness of specimens on longitudinal and transverse sections as a function of the annealing temperature. There is no obvious reduction in hardness until the annealing temperature up to 400 °C although the recovery exists in the range of annealing temperature.

This can be attributed to the possible precipitation hardening because some solute atoms can dissolve into the Cu matrix during heavy drawing and precipitate during annealing treatment at 200–400 °C [33–36]. As the annealing temperature increases above 400 °C, the hardness noticeably decreases because the recrystallization removes the work hardening.

The change of crystal orientation in heavy drawing strain may cause the variation of material properties [37]. Therefore, the change of crystal orientation in Cu ribbons in heavy drawing results in the different hardness values determined on longitudinal and transverse sections. With the annealing temperature increasing, the difference in hardness determined on longitudinal and transverse sections decreases. In particular, as the annealing temperature increases to higher than 500 °C, the recrystallization results in the annihilation of the hardness difference because the initial crystal orientation formed in heavy drawing is completely removed by the formation and propagation of equiaxed grains.

3.4. DSC

Fig. 6 shows the heat flow of the calorimeter in an experiment starting at 40 °C. The DSC curve shows exothermic reaction points in the positive *y*-direction. As for deformed pure metals, only the exothermal peak was observed and corresponded to the release of the stored energy during recrystallization [19,26,38]. However, in heavily drawn Cu–0.4 wt.%Cr–0.12 wt.%Zr–0.02 wt.%Si–0.05 wt.%Mg, the DSC result seems to be more complex. The curve includes two initial endothermal peaks and a subsequent exothermal peak as the temperature is lower than 380 °C. The initial endothermal peaks can be attributed to the dissolution of the solute clusters formed in dislocation walls at low temperatures [19]. The subsequent exothermal peak can be associated with the annihilation of some defects and the precipitation of some secondary particles during recovery. Only one large exothermal peak is observed at high temperatures and corresponds to the sufficient release of the

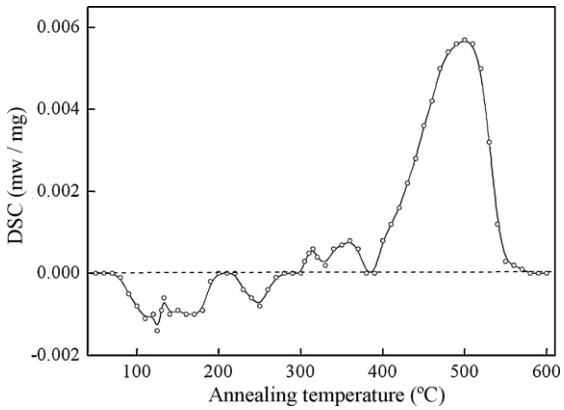

Fig. 6. Heat flow difference of two consecutive runs at 20 °C/min for Cu–0.4 wt.%Cr–0.12 wt.%Zr–0.02 wt.%Si–0.05 wt.%Mg drawn to $\eta = 6.0$.

Table 1
The measured E_s for the alloy annealed at different annealing temperatures.

Annealing temperature (°C)	390	400	450	500	550	600
E_s (J/mol)	37.4	35.6	29.1	12.2	0.191	0

stored energy during recrystallization when dislocation density significantly decreases.

The stored energy released by the recrystallization at different temperatures can be obtained by calculating the area under the large exothermal peak. The stored energy released sufficiently during recrystallization is measured to be 37.4 J/mol by integrating the DSC curve from 390 to 600 °C. After annealing treatment at different temperatures, the energy still stored in the alloy E_s is the difference between 37.4 J/mol and the stored energy released at different temperatures by the recrystallization. Table 1 shows the measured E_s for the alloy annealed at different temperatures.

In ultrafine-grained and nanocrystalline metals, the majority of stored energy released during recrystallization is attributed to the disappearance of high density grain boundaries and dislocations. The contributions from other defects such as vacancies and the associated elastic strain energy are minor [23–25]. The possible contribution from grain boundaries to the recrystallization exotherm can be estimated as follows. The total surface energy per unit volume attributing to grain boundaries E_{gb} is given as $2\nu/D$, where ν is grain boundary energy per unit area, D ribbon size. Taking ν as 0.6 J/m^2 for Cu [23–25,39] and D as 530 nm for as-drawn sample, the grain boundary energy contributing to the stored energy is 2.2×10^6 J/m^3 or 15.7 J/mol. Table 2 shows the measured E_{gb} for the alloy annealed at different temperatures. At higher temperature, grains have been coarsened obviously and then the grain boundary energy can be neglected.

In heavily drawn alloy, strength can be well correlated to the dislocation density using Taylor approach which strengthening is mainly caused by dislocation–dislocation interactions [25,40,41]. The flow stress σ can be related to the dislocation density by

$$\sigma = \sigma_o + \alpha MGb\rho^{1/2} \quad (4)$$

Table 2
The measured E_{gb} for the alloy annealed at different annealing temperatures.

Annealing temperature (°C)	Ribbon size (μm)	E_{gb} (J/mol)
300	0.530	15.7
400	0.610	14.3
450	0.800	10.8
500	1.53	5.60

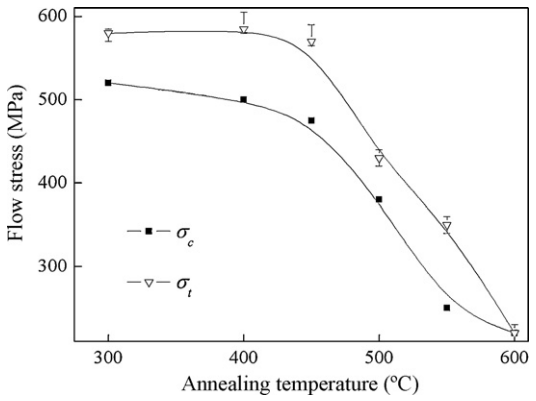

Fig. 7. The calculated flow stress σ_c and the measured flow stress σ_t dependent on the annealing temperature for Cu–0.4 wt.%Cr–0.12 wt.%Zr–0.02 wt.%Si–0.05 wt.%Mg.

where σ_o is the friction stress, M the Taylor factor ($M = 3$ for polycrystalline materials [41]), α a dimensionless number ($\alpha \approx 1/3$ is taken [25]), G the shear modulus ($G = 47$ GPa for Cu [41]) and b the Burgers vector ($b = 0.256$ nm in Cu lattice [41]). The dislocation density can be related to the stored energy in terms of $\rho = (E_s - E_{gb})/E_d$, where E_d is the energy per unit length of a dislocation and an average value of 5×10^{-9} J/m is taken without making any distinction between edge or screw dislocations, complete or partial dislocations [23,25].

If it is supposed that the dislocation density can be ignored in the alloy after full annealing, we can take the flow stress 220 MPa of the specimens annealed at 600 °C as the value of the friction stress σ_o in the investigation. Fig. 7 shows σ_c and σ_t dependent on the annealing temperature for Cu–0.4 wt.%Cr–0.12 wt.%Zr–0.02 wt.%Si–0.05 wt.%Mg, where σ_c is the flow stress obtained by Eq. (4) and σ_t is the flow stress measured by tensile test. In general, there is a similar change trend between the calculated values and the measured data with a stress difference of 40–90 MPa. It indicates the dislocation interactions play a dominant role and the grain refinement plays a minor role in strengthening effect for Cu–0.4 wt.%Cr–0.12 wt.%Zr–0.02 wt.%Si–0.05 wt.%Mg alloy. As the annealing temperature rises, both σ_c and σ_t decreases rapidly and σ_t is always higher than σ_c. For example, σ_t is 580 MPa higher than σ_c (520 MPa) at 300 °C. It may implies the strengthening effect of about 60 MPa is attributed to the grain refinement.

The changes of resistivity and dislocation density dependent on annealing temperature are shown in Fig. 8. In low temperature, the

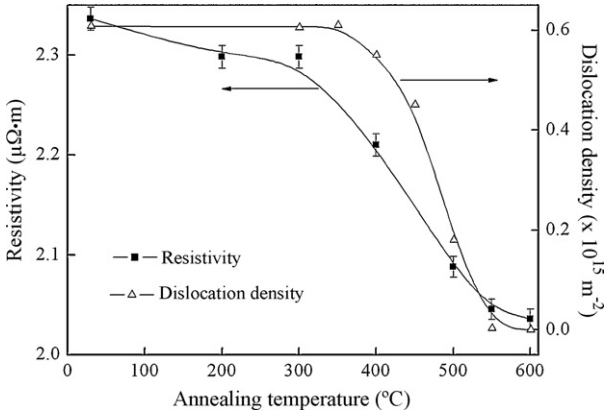

Fig. 8. Resistivity and dislocation density dependent on annealing temperature for the tested Cu–0.4 wt.%Cr–0.12 wt.%Zr–0.02 wt.%Si–0.05 wt.%Mg alloy.

dislocation density hardly changes, while the resistivity decreases with the annealing temperature increasing. This difference may be attributed to the annihilation of lattice defects such as point defects at low temperature [42,43]. In high temperature, there is a similar change trend between the resistivity and dislocation density. When the annealing temperature reaches 600 °C, the resistivity seems to be saturated, corresponding to the maximum decrease of dislocation density. The contribution of dislocations to the resistivity is in principle independent of the details of the arrangement of the dislocation and it is much more sensitive to their overall density [18].

4. Conclusions

With the annealing temperature increasing, the ribbonlike Cu crystals are gradually replaced by gross equiaxed grains, resulting in the decrease of hardness, flow stress and electrical resistivity.

The crystal orientation of as-drawn specimen is gradually approaching that of full annealed specimen and the hardness difference between longitudinal and transverse directions decreases as annealing temperature increasing.

The release of stored energy and the reduction of resistivity are primarily due to the decrease of dislocation density. The main strengthening effect is attributed to dislocation mechanism in Cu–0.4 wt.%Cr–0.12 wt.%Zr–0.02 wt.%Si–0.05 wt.%Mg alloy.

Acknowledgment

The project is supported by the National Science and Technology Pillar Program of China (Grant No. 2009BAG12A09).

References

[1] D.L. Zhang, K. Mihara, S. Tsubokawa, H.G. Suzuki, Mater. Sci. Technol. 16 (2000) 357–363.
[2] W.X. Qi, J.P. Tu, F. Liu, Y.Z. Yang, N.Y. Wang, H.M. Lu, X.B. Zhang, S.Y. Guo, M.S. Liu, Mater. Sci. Eng. A 343 (2003) 89–96.
[3] S.G. Mu, F.A. Guo, Y.Q. Tang, X.M. Cao, M.T. Tang, Mater. Sci. Eng. A 475 (2008) 235–240.
[4] P. Marmy, J. Nucl. Mater. 329A (2004) 188–192.
[5] U. Holzwarth, H. Stamm, J. Nucl. Mater. 279 (2000) 31–45.
[6] J.Q. Deng, X.Q. Zhang, S.Z. Shang, F. Liu, Z.X. Zhao, Y.F. Ye, Mater. Des. 30 (2009) 4444–4449.
[7] H.T. Zhou, J.W. Zhong, X. Zhou, Z.K. Zhao, Q.B. Li, Mater. Sci. Eng. A 498 (2008) 225–230.
[8] J.H. Su, Q.M. Dong, P. Liu, H.J. Li, B.X. Kang, Mater. Sci. Eng. A 392 (2005) 422–426.
[9] F.X. Huang, J.S. Ma, H.L. Ning, Z.T. Geng, C. Lu, S.M. Guo, X.T. Yu, T. Wang, H. Li, H.F. Lou, Scripta Mater. 48 (2003) 97–102.
[10] C.A. Poblano-Salas, J.D.O. Barceinas-Sanchez, J. Alloys Compd. 485 (2009) 340–345.
[11] C. Watanabe, R. Monzen, K. Tazaki, J. Mater. Sci. 43 (2008) 813–819.
[12] A. Vinogradov, V. Patlan, Y. Suzuki, K. Kitagawa, V.I. Kopylov, Acta Mater. 50 (2002) 1639–1651.
[13] C.T. Kwok, P.K. Wong, H.C. Man, F.T. Cheng, J. Nucl. Mater. 394 (2009) 52–62.
[14] M.M. Li, M.A. Sokolov, S.J. Zinkle, J. Nucl. Mater. 393 (2009) 36–46.
[15] D.J. Edwards, B.N. Singh, J.B. Bilde-Sorensen, J. Nucl. Mater. 342 (2005) 164–178.
[16] S. Tahtinen, M. Pyykkonen, P. Karjalainen-Roikonen, B.N. Singh, P. Toft, J. Nucl. Mater. 258 (1998) 1010–1014.
[17] S.A. Fabritsiev, A.S. Pokrovsky, D.J. Edwards, S.J. Zinkle, J. Nucl. Mater. 258 (1998) 1015–1021.
[18] M.B.D. Bever, L. Holt, A.L. Titchener, Prog. Mater. Sci. 17 (1972) 5–177.
[19] M. Verdier, I. Groma, L. Flandin, J. Lendvai, Y. Brechet, P. Guyot, Scripta Mater. 37 (1997) 449–454.
[20] V.L. Niranjani, K.C. Hari Kumar, V. Subramanya Sarma, Mater. Sci. Eng. A 515 (2009) 169–174.
[21] L. Liu, I. Baker, Scripta Mater. 28 (1993) 197–200.
[22] Y. Zhang, J.T. Wang, C. Cheng, J.Q. Liu, J. Mater. Sci. 43 (2008) 7326–7330.
[23] A. Rohatgi, K.S. Vecchio, Mater. Sci. Eng. A 328 (2002) 256–266.
[24] A. Rohatgi, K.S. Vecchio, G.T. Gray, Acta Mater. 49 (2001) 427–438.
[25] Y. Zhang, N.R. Tao, K. Lu, Acta Mater. 56 (2008) 2429–2440.
[26] F. Scholz, J.H. Driver, E. Woldt, Scripta Mater. 40 (1999) 949–954.
[27] G. Veltl, B. Scholz, H.D. Kunze, Mater. Sci. Eng. A 134 (1991) 1410–1413.
[28] I. Baker, L. Liu, D. Mandal, Scripta Mater. 32 (1995) 167–171.
[29] F.K. Lotgering, J. Inorg. Nucl. Chem. 9 (1959) 113.
[30] F. Dalla Torre, R. Lapovok, J. Sandlin, P.E. Thomson, C.H.J. Davies, E.V. Pereloma, Acta Mater. 52 (2004) 4819–4832.
[31] J.Y. Huang, Y.K. Wu, H.Q. Ye, Acta Mater. 44 (1996) 1211–1221.
[32] L.H. Qian, S.C. Wang, Y.H. Zhao, K. Lu, Acta Mater. 50 (2002) 3425–3434.
[33] S.I. Hong, M.A. Hill, Mater. Sci. Eng. A 264 (1999) 151–158.
[34] Y.S. Kim, J.S. Song, S.I. Hong, J. Mater. Process. Technol. 130 (2002) 278–282.
[35] M.S. Lim, J.S. Song, S.I. Hong, J. Mater. Sci. 35 (2000) 4557–4561.
[36] J.B. Liu, L. Meng, Mater. Sci. Eng. A 418 (2006) 320–325.
[37] T. Tsuru, Y. Shibutani, Phys. Rev. B 75 (2007) 035415.
[38] C.F. Gu, C.H.J. Davies, Mater. Sci. Eng. A 527 (2010) 1791–1799.
[39] L.E. Murr, Interfacial Phenomena in Metals and Alloys, Addison-Wesley, Reading, MA, 1975.
[40] A. Godfrey, W.Q. Cao, N. Hansen, Q. Liu, Metall. Mater. Trans. A 36 (2005) 2371–2378.
[41] J. Gubicza, N.Q. Chinh, G. Krallics, I. Schiller, T. Ungar, Curr. Appl. Phys. 6 (2006) 194–199.
[42] H. Margolin, Recrystallization, Grain Growth and Textures, American Society for Metals, Metals Park, OH, 1965.
[43] E. Schafler, G. Steiner, E. Korznikova, M. Kerber, M.J. Zehetbauer, Mater. Sci. Eng. A 410 (2005) 169–173.